

# Journal of Materials Chemistry A

Accepted Manuscript



This is an *Accepted Manuscript*, which has been through the Royal Society of Chemistry peer review process and has been accepted for publication.

*Accepted Manuscripts* are published online shortly after acceptance, before technical editing, formatting and proof reading. Using this free service, authors can make their results available to the community, in citable form, before we publish the edited article. We will replace this *Accepted Manuscript* with the edited and formatted *Advance Article* as soon as it is available.

You can find more information about *Accepted Manuscripts* in the [Information for Authors](#).

Please note that technical editing may introduce minor changes to the text and/or graphics, which may alter content. The journal's standard [Terms & Conditions](#) and the [Ethical guidelines](#) still apply. In no event shall the Royal Society of Chemistry be held responsible for any errors or omissions in this *Accepted Manuscript* or any consequences arising from the use of any information it contains.

## COMMUNICATION

## Fe<sub>3</sub>O<sub>4</sub>/Carbon quantum dots hybrid nanoflowers for highly active and recyclable visible-light driven photocatalyst

Cite this: DOI:  
10.1039/x0xx00000x

Received 00th January 2012,  
Accepted 00th January 2012

DOI: 10.1039/x0xx00000x

www.rsc.org/

Hui Wang,<sup>a</sup> Zengyan Wei,<sup>b</sup> Hiroshi Matsui,<sup>b</sup> and Shuiqin Zhou<sup>\*a</sup>

**Water dispersible Fe<sub>3</sub>O<sub>4</sub>@carbon quantum dots (CQDs) hybrid nanoflowers show highly efficient photocatalytic activities because of their strong absorption in visible light range and upconversion photoluminescence. The magnetic Fe<sub>3</sub>O<sub>4</sub> nanocrystals not only allow an efficient magnetic separation and recycling of the photocatalyst, but also promote the photocatalytic activities of the CQDs.**

Organic pollutants such as dyes and additives from industrial wastewater have generated great concern with their potential carcinogenic, mutagenic and bactericide properties in the past decades.<sup>1</sup> Among various sequestration strategies, photocatalytic degradation of organic compounds is a compelling approach due to their relatively low operation costs without second time pollution.<sup>2</sup> A major challenge is to find potent photocatalysts for such a task. A good photocatalyst should be able to utilize natural visible light and be photostable, inexpensive, and nontoxic. Nanoscale wide-band-gap semiconductors and oxoacid salt have been recently developed for photodegradation of dyes. However, they usually require UV light excitation.<sup>3,4</sup> In order to achieve visible light driven photodegradation of organics, various hetero or composite-structured semiconductors and silica quantum dots have been developed for photocatalysts.<sup>5</sup> In particular, the carbon coated or graphene composited nanostructures could significantly enhance the photocatalytic activity of these semiconductor nanoparticles.<sup>3a,5b</sup> Recent study shows that photoactive carbon quantum dots (CQDs) are both excellent electron donors and excellent electron acceptors.<sup>6</sup> Compared to conventional semiconductor quantum dots, CQDs not only display low-toxicity and eco-friendliness, but also exhibit broad absorption spectrum, large absorption coefficient, upconversion luminescence properties, and good solubility in polar solvents.<sup>7</sup> These properties endow CQDs great opportunities to be used as a new class of photocatalysts.<sup>8</sup> The upconversion luminescence properties are especially attractive because the CQDs can emit low-wavelength light under the excitation of long wavelength light, which enable the CQD-based photocatalysts workable under visible light induction.<sup>9</sup> On the other hand, from a practical point of view, the application and recycling of photocatalysts require an additional separation step from the reaction solution, which can be a largish

expense. It is highly desirable to develop photocatalysts that can be easily collected for re-use. Magnetic iron oxide nanoparticles can be collected easily by an external magnetic field, and hence have advantages as a carrier to facilitate separation and recycling of nanomaterials in aqueous solutions.<sup>10</sup> Therefore, it remains an important challenge to synthesize a kind of photocatalysts that can combine the merits of CQDs as photocatalysts and magnetic recyclability of iron oxide nanoparticles.

Herein, we report a facile route for one-pot solvothermal preparation of highly dispersible and highly active photocatalysts for degradation of organic dyes under visible light, based on the hybrid nanoflowers (NFs) composed of superparamagnetic iron oxide (Fe<sub>3</sub>O<sub>4</sub>) nanocrystals clustered in the core and fluorescent CQDs assembled on the surface of the Fe<sub>3</sub>O<sub>4</sub> nanocrystals. The water-dispersible Fe<sub>3</sub>O<sub>4</sub>@CQDs hybrid NFs were synthesized through an improved one-pot solvothermal method with ferrocene as precursor in the presence of hydrogen peroxide (H<sub>2</sub>O<sub>2</sub>).<sup>11</sup> H<sub>2</sub>O<sub>2</sub> is important and necessary for the fabrication of Fe<sub>3</sub>O<sub>4</sub>@CQDs hybrid NFs. Without addition of H<sub>2</sub>O<sub>2</sub>, no product could be obtained under the same reaction conditions. The formation of Fe<sub>3</sub>O<sub>4</sub>@CQDs hybrid NFs in the reaction medium should involve very complicated chemical process. The role of H<sub>2</sub>O<sub>2</sub> could be briefly explained as follows. In the sealed reactor containing ferrocene and H<sub>2</sub>O<sub>2</sub> dissolved in acetone (with some water from H<sub>2</sub>O<sub>2</sub> aqueous solution) at 200°C, the ferrocene quickly decomposes to form iron and cyclopentadiene. The chemical bonds of C-H in the cyclopenta-1,3-diene are ruptured, leading to the formation of carbon-based free radicals. These small carbon free radicals can form relatively large carbon-based fragments or CQDs under the high reaction temperature and high pressure from the gasification of acetone and water in reactor. Meanwhile, the O<sub>2</sub> decomposed from the H<sub>2</sub>O<sub>2</sub> can oxidize the Fe atoms to form Fe<sup>2+</sup> and iron oxide. The presence of Fe<sup>2+</sup> in turn catalyze the decomposition of H<sub>2</sub>O<sub>2</sub> to form highly reactive free radicals such as hydroxyl HO· and hydroperoxyl HOO· and form more gaseous O<sub>2</sub> and H<sub>2</sub>O. These highly reactive free radicals can speed up the oxidation of Fe to form iron oxide nanocrystals and rapidly react with the carbon fragment free radicals to form the hydrophilic hydroxyl and carboxyl groups. On the other hand, the produced gaseous O<sub>2</sub> and H<sub>2</sub>O can further increase the pressure of the reaction medium, which in turn help the reaction of

carbon-based free radicals to form highly crystallized CQDs. The as-prepared  $\text{Fe}_3\text{O}_4@\text{CQDs}$  hybrid NFs demonstrates excellent photoluminescent (PL) properties including excitation ( $\lambda_{\text{ex}}$ ) tunable emission, upconversion PL, and excellent photostability. The absorption in visible light range with a broad band at 556 nm and upconversion PL remarkably improves the photocatalytic activity of the  $\text{Fe}_3\text{O}_4@\text{CQDs}$  hybrid NFs for the degradation of methylene blue (MB) dye molecules under visible light. The magnetic  $\text{Fe}_3\text{O}_4$  nanocrystals in the core not only allow an efficient separation, purification, and recycling of the photocatalyst by simply applying an external magnetic field, but also promote the photocatalytic function of the CQDs. The excellent dispersibility of the  $\text{Fe}_3\text{O}_4@\text{CQDs}$  hybrid NFs in water enables the photoreduction of dye molecules under essentially a homogeneous reaction condition.

A series of  $\text{Fe}_3\text{O}_4@\text{CQDs}$  hybrid NFs were synthesized by adding different amount of 30%  $\text{H}_2\text{O}_2$  aqueous solution into the autoclaves holding the same amount of precursor ferrocene and solvent acetone. Specifically, 3.0, 4.5, and 6.0 ml of  $\text{H}_2\text{O}_2$  solution were respectively used. The resultant samples were coded as  $\text{Fe}_3\text{O}_4@\text{CQDs}$ -3.0,  $\text{Fe}_3\text{O}_4@\text{CQDs}$ -4.5, and  $\text{Fe}_3\text{O}_4@\text{CQDs}$ -6.0, correspondingly. The crystallographic structure and phase purity of the as-prepared samples were examined by X-ray powder diffraction (XRD) and Raman scattering techniques. The observed reflections of 220, 311, 400, 422, 511, 440 in the typical XRD patterns [Fig. S1a in the Electronic Supplementary Information (ESI)] can be indexed to the magnetic  $\text{Fe}_3\text{O}_4$  nanocrystals. In typical Raman scattering patterns (Fig. S1b in the ESI), the peak at around  $1583\text{ cm}^{-1}$  involves the in-plane bond stretching motion of  $\text{sp}^2$ -hybridized carbon atoms in a two-dimensional hexagonal lattice, which also exists as the G mode with the  $E_{2g}$  symmetry.<sup>12a</sup> The D mode of graphite around  $1371\text{ cm}^{-1}$  is related to the vibrations of carbon atoms with dangling bonds in the termination plane of disordered graphite or glassy carbon.<sup>12b</sup> It is interesting to note that the intensity ratio of G-band to D-band ( $I_G/I_D$ ) in the Raman scattering curves of the  $\text{Fe}_3\text{O}_4@\text{CQDs}$  hybrid NFs increases with the increase in the amount of  $\text{H}_2\text{O}_2$  presented in the synthetic reaction medium, suggesting that the high feeding of  $\text{H}_2\text{O}_2$  is necessary to produce crystallographic CQDs. The  $I_G/I_D$  ratios for the  $\text{Fe}_3\text{O}_4@\text{CQDs}$ -3.0,  $\text{Fe}_3\text{O}_4@\text{CQDs}$ -4.5, and  $\text{Fe}_3\text{O}_4@\text{CQDs}$ -6.0 hybrid NFs are 1.24, 1.25, and 1.32, respectively. The high  $I_G/I_D$  ratios suggest that these hybrid NFs contain much more crystalline graphitic CQDs than the amorphous carbon. Fig. S1c shows the FT-IR spectrum of the  $\text{Fe}_3\text{O}_4@\text{CQDs}$ -6.0 hybrid NFs. The sharp absorption peak at  $1710\text{ cm}^{-1}$  can be attributed to the C=O stretching of the carboxylic acid groups conjugated with condensed aromatic carbons, while the broad absorption around  $3408\text{ cm}^{-1}$  should be from the -OH groups.<sup>13</sup> These hydrophilic functional groups enable the resultant  $\text{Fe}_3\text{O}_4@\text{CQDs}$  hybrid NFs to be dispersed in aqueous media very well. Fig. S1d shows typical UV-Vis absorption spectra of the  $\text{Fe}_3\text{O}_4@\text{CQDs}$  hybrid NFs in the visible light region. A broad band at about 556 nm could be clearly observed for samples synthesized with high content of  $\text{H}_2\text{O}_2$ , although the overall absorption intensity in visible light region is weaker than the sharp absorption peak at 244 nm originated from the multiple polyaromatic chromophores (Fig. S2 in the ESI).<sup>13</sup> The strong absorption in the visible light region is important for the resultant hybrid NFs to be used for photodegradation of organics under visible light irradiation.

The morphology and structures of the resultant  $\text{Fe}_3\text{O}_4@\text{CQDs}$  hybrid NFs are further elucidated by transmission electron microscopy (TEM). Fig. 1a manifests that the  $\text{Fe}_3\text{O}_4@\text{CQDs}$ -6.0 hybrid NFs are nearly uniform in size and shape with an average diameter of 100 nm. The TEM image of an individual  $\text{Fe}_3\text{O}_4@\text{CQDs}$  hybrid NF (Fig. 1b) further reveals that the flower-like particle is composed of  $\text{Fe}_3\text{O}_4$  nanocrystals clustered in the core region and

CQDs assembled on their surface. Fig. 1c displays a high-resolution TEM (HRTEM) image of the sectional hybrid NF showing a single CQD and  $\text{Fe}_3\text{O}_4$  nanocrystal. It can be seen that both the  $\text{Fe}_3\text{O}_4$  nanocrystal particle ( $\sim 20\text{ nm}$ ) and the crystallographic CQD ( $\sim 17\text{ nm}$ ) have a clear lattice fringe. From the 2D lattice fringes of the CQDs, an interplanar distance about  $0.335\text{ nm}$  is determined, which corresponds to the (006) lattice planes of the graphitic ( $\text{sp}^2$ ) carbon. To further confirm the compositions of the nanocrystals in the inner core and outer shell of the hybrid NFs, energy dispersive analysis of X-ray were conducted. The energy dispersive spectrum (EDS) of the single crystal on the outer shell (Fig. 1d) only reveals the presence of C and Cu elements. Because the Cu is from the copper grid for TEM sample preparation, this result indicates that the nanocrystals in the shell only contain carbon. In contrast, the EDS of the nanocrystal in the inner core (Fig. 1e) shows the existence of Fe, O, C, and Cu elements. While the Cu is from the copper grid, the Fe, O, and C should be attributed to the magnetic  $\text{Fe}_3\text{O}_4$  nanocrystals clustered in the carbon matrix. The HRTEM and EDS results of the  $\text{Fe}_3\text{O}_4@\text{CQDs}$ -3.0 and  $\text{Fe}_3\text{O}_4@\text{CQDs}$ -4.5 (Fig. S3 and S4) show similar results, except that the crystallinity of the  $\text{Fe}_3\text{O}_4$  nanocrystals and CQDs in  $\text{Fe}_3\text{O}_4@\text{CQDs}$ -3.0 is relatively lower than that in  $\text{Fe}_3\text{O}_4@\text{CQDs}$ -4.5 and  $\text{Fe}_3\text{O}_4@\text{CQDs}$ -6.0 samples. Combining all these analytical results on the hybrid NFs, it is reasonable to conclude that the  $\text{Fe}_3\text{O}_4@\text{CQDs}$  NFs are composed of iron oxide nanocrystals clustered in the core and crystallographic CQDs assembled on the surface as shell.

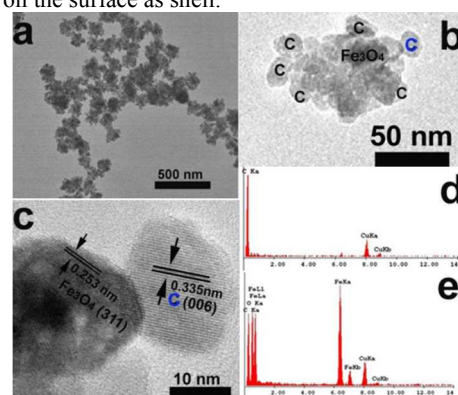


Fig. 1. (a and b) TEM images of the  $\text{Fe}_3\text{O}_4@\text{CQDs}$ -6.0 hybrid NFs; (c) High resolution TEM image of the sectional hybrid NF in Fig. 1b, showing single CQD and  $\text{Fe}_3\text{O}_4$  nanocrystals; (d) and (e) Energy dispersive spectrum of the single CQD and  $\text{Fe}_3\text{O}_4$  nanocrystal, respectively.

To further explore the optical properties of the  $\text{Fe}_3\text{O}_4@\text{CQDs}$  NFs, a detailed PL study was carried out under different excitation wavelengths. Fig. 2a shows the evolution of PL spectra of the  $\text{Fe}_3\text{O}_4@\text{CQDs}$ -6.0 NFs obtained with excitation light wavelength increasing from 240 nm to 460 nm. The emission peak gradually shifts to longer wavelength and increases its strength until reaching the maximum intensity at 547 nm obtained with an excitation wavelength of 460 nm, which indicate a distribution of the different surface energy traps of the CQDs.<sup>15</sup> The PL quantum yield of the  $\text{Fe}_3\text{O}_4@\text{CQDs}$ -6.0 sample was determined to be 9.8%. Fig. 2b shows the PL spectra of the  $\text{Fe}_3\text{O}_4@\text{CQDs}$ -6.0 NFs excited by long-wavelength light from 960 to 500 nm, which clearly demonstrate the upconverted emissions from 560 to 390 nm. The upconversion PL property of the  $\text{Fe}_3\text{O}_4@\text{CQDs}$  NFs can be attributed to the multiphoton active process similar to the previously reported carbon dots.<sup>9a,16</sup> The samples of  $\text{Fe}_3\text{O}_4@\text{CQDs}$ -3.0 and  $\text{Fe}_3\text{O}_4@\text{CQDs}$ -4.5 hybrid NFs synthesized with less amount of  $\text{H}_2\text{O}_2$  demonstrate similar PL properties (Fig. S5 and S6), including excitation wavelength ( $\lambda_{\text{ex}}$ ) tunable emissions and upconversion PL. One

difference is that the  $\text{Fe}_3\text{O}_4@\text{CQDs}$ -6.0 NFs shows the maximum PL intensity at a much longer wavelength than  $\text{Fe}_3\text{O}_4@\text{CQDs}$ -3.0 and  $\text{Fe}_3\text{O}_4@\text{CQDs}$ -4.5 NFs, which might be attributed to the higher crystallinity of the CQDs formed in the  $\text{Fe}_3\text{O}_4@\text{CQDs}$ -6.0 sample.

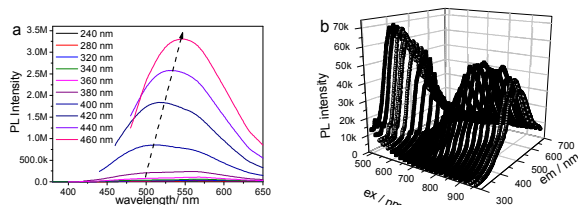


Fig. 2. (a) PL spectra and (b) upconverted PL spectra of the  $\text{Fe}_3\text{O}_4@\text{CQDs}$ -6.0 hybrid NFs obtained with different excitation wavelengths.

Given the excellent optical properties, the photocatalytic activity of the  $\text{Fe}_3\text{O}_4@\text{CQDs}$  hybrid NFs was evaluated for the degradation of methylene blue (MB) dye molecules under visible-light irradiation. As shown in the photos of Fig. 3a, the color of the bright blue MB solution (0.001 M, 3.0 mL) can completely disappear after adding 1 mg of  $\text{Fe}_3\text{O}_4@\text{CQDs}$ -6.0 NFs for 15 min under visible light irradiation, revealing that the  $\text{Fe}_3\text{O}_4@\text{CQDs}$ -6.0 hybrid NFs are highly efficient catalysts for photodegradation of MB. Fig. 3 also compares the time dependent photodegradation profiles of MB in the presence of different catalysts under 75W Xenon lamp with a cut off at 420 nm for visible light (a) and without cut off for whole spectrum (b), respectively. Without the addition of  $\text{Fe}_3\text{O}_4@\text{CQDs}$  hybrid NFs, only slight reduction (< 5.4 %) of MB was observed for 30 min from Fig. 3. In contrast, the presence of the  $\text{Fe}_3\text{O}_4@\text{CQDs}$  hybrid NFs could significantly speed up the degradation of MB under the same conditions. For example, the  $\text{Fe}_3\text{O}_4@\text{CQDs}$ -6.0 hybrid NFs can degrade the MB molecules by 80% in 10 min for both Figures. These results indicate that catalysts of  $\text{Fe}_3\text{O}_4@\text{CQDs}$  NFs are necessary for efficient photodegradation of MB dye under visible light. The degradation fractions of MB in the presence of different photocatalysts are 79.7%, 88.4%, and 94.4% for  $\text{Fe}_3\text{O}_4@\text{CQDs}$ -3.0,  $\text{Fe}_3\text{O}_4@\text{CQDs}$ -4.5, and  $\text{Fe}_3\text{O}_4@\text{CQDs}$ -6.0, respectively, after the MB solution was exposed to visible light for 30 min (Fig. 3a). After removing the cutting off filter at 420 nm, the degradation fractions of MB in the presence of different photocatalysts under the whole spectrum light from the Xenon lamp for 30 min are 84.6%, 91.2%, and 95.8% for  $\text{Fe}_3\text{O}_4@\text{CQDs}$ -3.0,  $\text{Fe}_3\text{O}_4@\text{CQDs}$ -4.5, and  $\text{Fe}_3\text{O}_4@\text{CQDs}$ -6.0, respectively (Fig. 3b). The slightly higher photodegradation activity for MB of the  $\text{Fe}_3\text{O}_4@\text{CQDs}$  catalysts under the whole spectrum (without cut off) than under the visible light (cut off at 420 nm) should be attributed to the contribution of the small fraction of UV light from the whole spectrum of Xenon lamp. The gradually increased photocatalytic activity of the three catalysts may partially result from the enhanced  $\pi$ - $\pi$  attachment ability of the MB molecules on the highly crystallographic and conjugated CQDs assembled on the surface of the  $\text{Fe}_3\text{O}_4@\text{CQDs}$ -4.5 and  $\text{Fe}_3\text{O}_4@\text{CQDs}$ -6.0 samples. In terms of the amount of MB dye molecules degraded by per gram of photocatalyst in the same exposure time period under visible light, our  $\text{Fe}_3\text{O}_4@\text{CQDs}$  hybrid NFs exhibited much higher photocatalytic activity than the previously reported catalysts including P25-graphene,<sup>3a</sup>  $\text{Fe}_3\text{O}_4@\text{TiO}_2$  nanosheets,<sup>3c</sup>  $\text{C}_3\text{N}_4/\text{BiPO}_4$ ,<sup>4a</sup> and CNT-confined  $\text{TiO}_2$ .<sup>5h</sup> In order to understand the photocatalytic mechanism for the highly active  $\text{Fe}_3\text{O}_4@\text{CQDs}$  hybrid NFs, we did a control experiment. The  $\text{Fe}_3\text{O}_4$  nanocrystals in the core of the  $\text{Fe}_3\text{O}_4@\text{CQDs}$ -6.0 hybrid NFs were removed via acid-dissolution with the resultant hollow CQDs shell being coded as CQDs-6.0. As shown in Fig. 3a, only about 42.5 % of the MB was degraded by the CQDs-6.0 catalyst after 30 min under the same experimental conditions as the  $\text{Fe}_3\text{O}_4@\text{CQDs}$  hybrid

NFs catalysts. This much lower photocatalytic ability for MB degradation of the CQDs-6 than the  $\text{Fe}_3\text{O}_4@\text{CQDs}$  hybrid NFs indicates that the excellent photocatalytic activities of the  $\text{Fe}_3\text{O}_4@\text{CQDs}$  hybrid NFs should be attributed to the synergistic interaction of the shell CQDs with the  $\text{Fe}_3\text{O}_4$  nanocrystals in the core.

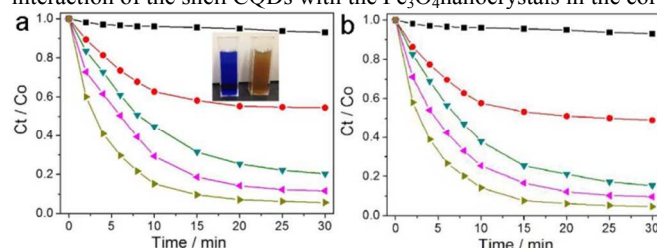


Fig. 3. The photodegradation profiles of MB under 75 W Xenon lamp (a) with a cut off 420 nm for visible light and (b) without cut off for the whole spectrum in the presence of different catalysts (■: control with no catalyst; ●: CQDs-6.0; ▼:  $\text{Fe}_3\text{O}_4@\text{CQDs}$ -3.0; ▲:  $\text{Fe}_3\text{O}_4@\text{CQDs}$ -4.5; ►:  $\text{Fe}_3\text{O}_4@\text{CQDs}$ -6.0), respectively. The inset in (a) shows the photos of MB aqueous solutions before and after the addition of  $\text{Fe}_3\text{O}_4@\text{CQDs}$ -6.0 NFs for 15 min.

Fig. 4 illustrated the possible mechanism for the photocatalytic degradation of MB upon the  $\text{Fe}_3\text{O}_4@\text{CQDs}$  hybrid NFs. When the  $\text{Fe}_3\text{O}_4@\text{CQDs}$  hybrid NFs were illuminated using visible light, the light with shorter wavelength (390 to 560 nm) will be emitted as a result of the upconversion PL property of the CQDs. These photoinduced light at the shorter wavelengths can in turn excite the  $\text{Fe}_3\text{O}_4$  nanocrystals to form electron/hole ( $e^-/h^+$ ) pairs.<sup>17</sup> These photon-excited electrons can be shuttled freely in the conducting network of CQDs due to their electron-storage capacity.<sup>6</sup> Additionally, the CQDs serving as electron reservoir can suppress the recombination of photogenerated electron-hole pairs.<sup>8c,9a</sup> The both produced electron/hole pairs react with the adsorbed oxidants/reducers (usually  $\text{O}_2/\text{OH}^-$ ) on the surface of the  $\text{Fe}_3\text{O}_4@\text{CQDs}$  hybrid NFs to produce active oxygen radicals (e.g.  $\cdot\text{O}_2^-$ ,  $\cdot\text{OH}$ ), which subsequently cause degradation of the MB dye molecules.<sup>18</sup> This mechanism is supported by the experimental evidence of the hydroxyl radicals ( $\cdot\text{OH}$ ) produced by the  $\text{Fe}_3\text{O}_4@\text{CQDs}$ -6.0 NFs photocatalyst under visible-light irradiation (Figure S7a). This mechanism is further supported by the experimental results that the presence of  $\text{N}_2$  purging, hole scavenger EDTA (1  $\mu\text{M}$ ), and a hydroxyl radical scavenger tBuOH (1  $\mu\text{M}$ ) can significantly reduce the photodegradation fraction of MB under the same conditions using the  $\text{Fe}_3\text{O}_4@\text{CQDs}$ -6.0 NFs as a catalyst (Figure S7b). This mechanism also explains why the photocatalytic activity of the  $\text{Fe}_3\text{O}_4@\text{CQDs}$ -3.0,  $\text{Fe}_3\text{O}_4@\text{CQDs}$ -4.5, and  $\text{Fe}_3\text{O}_4@\text{CQDs}$ -6.0 hybrid NFs for MB degradation gradually increases under visible light. As we discussed above for the HRTEM images (Fig. 1, Fig. S3, and Fig. S4), the crystallinity of the CQDs and  $\text{Fe}_3\text{O}_4$  nanocrystals gradually increases in the sequence of  $\text{Fe}_3\text{O}_4@\text{CQDs}$ -3.0,  $\text{Fe}_3\text{O}_4@\text{CQDs}$ -4.5, and  $\text{Fe}_3\text{O}_4@\text{CQDs}$ -6.0 hybrid NFs, which results in stronger absorption in visible light region and shorter wavelength of the emitted light. As shown in Fig. S1d, the absorption intensity in the visible light region (around 556 nm) gradually increases from  $\text{Fe}_3\text{O}_4@\text{CQDs}$ -3.0 to  $\text{Fe}_3\text{O}_4@\text{CQDs}$ -4.5, and then to  $\text{Fe}_3\text{O}_4@\text{CQDs}$ -6.0 sample. Furthermore, the upconversion PL light emitted from the  $\text{Fe}_3\text{O}_4@\text{CQDs}$ -3.0,  $\text{Fe}_3\text{O}_4@\text{CQDs}$ -4.5, and  $\text{Fe}_3\text{O}_4@\text{CQDs}$ -6.0 also gradually blue shifted to a shorter wavelength (Fig. S8) under the same excitation wavelength (556 nm). The stronger absorption in visible light region and shorter emitted light wavelength can in turn produce more electron/hole pairs on the hybrid NFs synthesized with higher amount of  $\text{H}_2\text{O}_2$ , thus lead to higher photocatalytic activities.

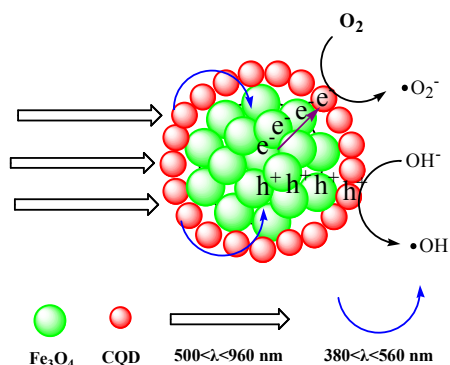


Fig. 4. Possible catalytic mechanism for Fe<sub>3</sub>O<sub>4</sub>@CQDs hybrid NFs under visible light.

The magnetic properties of the Fe<sub>3</sub>O<sub>4</sub>@CQDs hybrid NFs have been investigated using a superconducting quantum interference device (SQUID) magnetometer prior to the recycling experiments of photocatalysts. Fig. 5a shows a hysteresis loop of Fe<sub>3</sub>O<sub>4</sub>@CQDs-6.0 measured at 300 K in an applied magnetic field of up to 10000 Oe, which indicates that the saturation magnetization (M<sub>s</sub>) of the hybrid NFs is 33.8 emu/g. No obviously remanence or coercivity was observed at room temperature, indicating a superparamagnetic behavior of the hybrid NFs, which is essential for the magnetic separation and recycling of these NFs as photocatalysts. As demonstrated in the inset of Fig. 5a, the magnetic moment of the Fe<sub>3</sub>O<sub>4</sub> nanocrystals in the core is sufficiently high so that a complete separation of the catalyst colloids from solution can be achieved within 1 min under the induction of an external magnet (0.3 T). The separated catalyst from a reaction solution was repeatedly washed with deionized water and dried. The recovered catalyst can be then used for second run for the photodegradation of MB. Fig. 5b compares the catalytic performance of the Fe<sub>3</sub>O<sub>4</sub>@CQDs-6.0 hybrid NFs for five runs under the visible light with a cut off at 420 nm. The hybrid NFs demonstrate a remarkable photostability as the degradation percentage of MB only drops slightly after each reused cycle, which may result from the loss of small amount of catalysts during the recycling process of magnetic separation, washing, drying, and redispersion. Even so, the degradation fraction of MB based on the Fe<sub>3</sub>O<sub>4</sub>@CQDs-6.0 photocatalysts still reaches 91.6% after five runs. Fig. 5c compares the catalytic performance of the Fe<sub>3</sub>O<sub>4</sub>@CQDs-6.0 hybrid NFs under the whole spectrum light from xenon lamp for ten runs of catalytic reaction and recycling. Similarly, the catalyst demonstrated high stable photocatalytic activity with only a slight decrease in the degradation fraction of MB from 95.8% to 91.1% after ten repeated runs. This excellent photocatalytic stability of the catalysts should be attributed to the very stable nanostructures of the Fe<sub>3</sub>O<sub>4</sub>@CQDs hybrid NFs. As shown in Fig. S9, the recycled Fe<sub>3</sub>O<sub>4</sub>@CQDs-6.0 hybrid NFs after ten runs of catalytic reaction and recycling shows a similar structure to that of the as-synthesized hybrid NFs (Fig. 1a) with CQDs still combined on the surface of Fe<sub>3</sub>O<sub>4</sub> nanocrystals. These results show that the catalysts of Fe<sub>3</sub>O<sub>4</sub>@CQDs hybrid NFs can be recovered efficiently from the reaction solution by using external magnetic fields for repeated use.

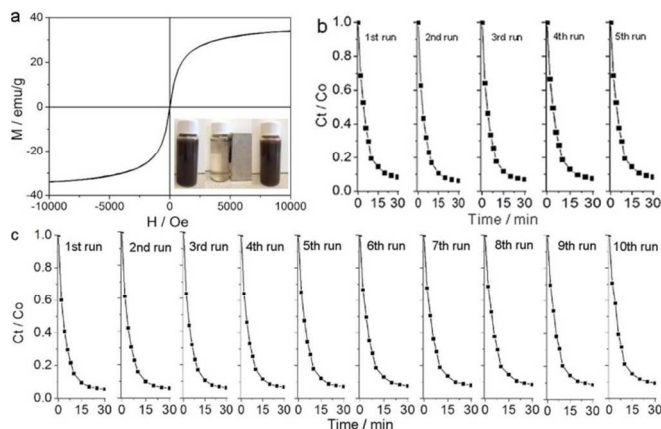


Fig. 5.(a) The hysteresis loop of Fe<sub>3</sub>O<sub>4</sub>@CQDs-6.0 NFs measured at room temperature. The inset shows the photographs of the aqueous dispersions of the hybrid NFs (left) without magnetic field, (middle) with magnetic field for 1 min, and (right) after the removal of magnetic field; (b,c) Multiple cycles of photodegradation profiles of MB as a function of reaction time *t* using the Fe<sub>3</sub>O<sub>4</sub>@CQDs-6.0 hybrid NFs as catalysts (b) five cycles under visible light from Xenon lamp with a cut off at 420 nm and (c) ten cycles under the whole spectrum from Xenon lamp without cut off, respectively.

In summary, we have demonstrated a facile one-pot solvothermal method to synthesize a series of highly stable and highly active photocatalysts of Fe<sub>3</sub>O<sub>4</sub>@CQDs hybrid NFs for degradation of organic dye under visible light. The flower-like nanostructure with the highly fluorescent CQDs (quantum yield about 9.8%) assembled on the surface of Fe<sub>3</sub>O<sub>4</sub> nanocrystals is essential for the excellent optical properties and high photocatalytic performance of the resultant Fe<sub>3</sub>O<sub>4</sub>@CQDs hybrid NFs. The hybrid NFs can be easily recovered by external magnetic field for repeated use. The combined stable dispersibility in water, magnetic recycling and targeting ability, upconverted PL properties, and excellent photostability of the Fe<sub>3</sub>O<sub>4</sub>@CQDs hybrid NFs provide a promising candidate for highly efficient, reusable, and visible-light driven photocatalysts in environmental remediation technology.

#### Acknowledgements

We gratefully acknowledge the financial support from American Diabetes Association (Basic Science Award 1-12-BS-243) and the PSC-CUNY Research Award (66076-00 44).

#### Notes and references

<sup>a</sup> Department of Chemistry, The College of Staten Island, and The Graduate Center, The City University of New York, Staten Island, NY 10314 USA. E-mail address: shuiqin.zhou@csi.cuny.edu; Tel.: +1 718 982 3897; Fax: +1 718 982 3910. A

<sup>b</sup> Department of Chemistry and Biochemistry, Hunter College, The City University of New York, New York, NY 10065, USA

† Electronic Supplementary Information (ESI) available: Experimental section, Fig. S1- Fig. S9. See DOI: 10.1039/b000000x/

1 (a) S. M. A. G. Ulson de Souza, E. Forgiarini and A. A. Ulson de Souza, *J. Hazard. Mater.*, 2007, **147**, 1073; (b) K. P. Sharma, S. Sharma, S. Sharma, P. K. Singh, S. Kumar, R. Grover and P. K. Sharma, *Chemosphere*, 2007, **69**, 48; (c) C. A. Martínez-Huitle and E. Brillas, *Appl. Catal., B: Environ.*, 2009, **87**, 105.

2 M. R. Hoffmann, S. T. Martin, W. Choi and D. W. Bahneman, *Chem. Rev.*, 1995, **95**, 69.

3 (a) H. Zhang, X. Lv, Y. Li, Y. Wang and J. Li, *ACS Nano*, 2010, **4**, 380; (b) H. Wu, H. H. Hng and X. Lou, *Adv. Mater.*, 2012, **24**, 2567; (c) J. S. Chen, C. Chen, J. Liu, R. Xu, S. Z. Qiao and X. Lou, *Chem. Commun.*, 2011, **47**, 2631; (d) C. Tian, Q. Zhang, A. Wu, M. Jiang, Z. Liang, B. Jiang and H. Fu, *Chem. Commun.*, 2012, **48**, 2858; (e) S. Chakrabarti and B. K. Dutta, *J. Hazard. Mater.*, 2004, **112**, 269; (f) R. Comparelli, E. Fanizza, M. L. Curri,

- P. D. Cozzoli, G. Mascolo and A. Agostiano, *Appl. Catal., B: Environ.*, 2005, **60**, 1; (g) N. M. Kinsinger, A. Dudchenko, A. Wong and D. Kisailus, *ACS Appl. Mater. Interfaces*, 2013, **5**, 6247; (h) S. Balachandran, M. Swaminathan, *J. Phys. Chem. C*, 2012, **116**, 26306.
- 4 (a) C. Pan, J. Xu, Y. Wang, D. Li and Y. Zhu, *Adv. Funct. Mater.*, 2012, **22**, 1518; (b) C. Pan and Y. Zhu, *Environ. Sci. Technol.*, 2010, **44**, 5570.
- 5 (a) W. Yang, L. Zhang, Y. Hu, Y. Zhong, H. Wu and X. Lou, *Angew. Chem. Int. Ed.*, 2012, **51**, 11501; (b) Y. Hu, X. Gao, L. Yu, Y. Wang, J. Ning, S. Xu and X. Lou, *Angew. Chem. Int. Ed.*, 2013, **52**, 5636; (c) Y. Hu, Y. Liu, H. Qian, Z. Li and J. Chen, *Langmuir*, 2010, **26**, 18570; (d) X. Li, S. Ouyang, N. Kikugawa and J. Ye, *Appl. Catal., A: Gener.*, 2008, **334**, 51; (e) B. Subash, B. Krishnakumar, M. Swaminathan and M. Shanthi, *Langmuir*, 2013, **29**, 939; (f) Z. H. Kang, C. H. A. Tsang, N. B. Wong, Z. D. Zhang and S. T. Lee, *J. Am. Chem. Soc.*, 2007, **129**, 12090; (g) M. Zhou, Y. Hu, Y. Liu, W. Yang and H. Qian, *CrystEngComm*, 2012, **14**, 7686; (h) W. Chen, Z. Fan, B. Zhang, G. Ma, K. Takanabe, X. Zhang and Z. Lai, *J. Am. Chem. Soc.*, 2011, **133**, 14896; (i) Y. Hou, X. Li, Q. Zhao, X. Quan and G. H. Chen, *Adv. Funct. Mater.*, 2010, **20**, 2165; (j) M. Wang, L. Sun, Z. Lin, J. Cai, K. Xie and C. Lin, *Energy Environ. Sci.*, 2013, **6**, 1211; (k) Y. Zheng, C. Chen, Y. Zhang, X. Lin, Q. Zheng, K. Wei and J. Zhu, *J. Phys. Chem. C*, 2008, **112**, 10773.
- 6 X. Wang, L. Cao, F. S. Lu, M. J. Meziani, H. T. Li, G. Qi, B. Zhou, B. A. Harruff, F. Kermarrec and Y. P. Sun, *Chem. Commun.*, 2009, 3774.
- 7 (a) A. B. Bourlinos, A. Stassinopoulos, D. Anglos, R. Zboril, M. Karakassides and E. P. Giannelis, *Small*, 2008, **4**, 455; (b) X. Y. Xu, R. Ray, Y. L. Gu, H. J. Ploehn, L. Gearheart, K. Raker and W. A. Scriven, *J. Am. Chem. Soc.*, 2004, **126**, 12736.
- 8 (a) L. Cao, S. Sahu, P. Anilkumar, C. E. Bunker, J. Xu, K. A. S. Fernando, P. Wang, E. A. Guliants, K. N. Tackett and Y.-P. Sun, *J. Am. Chem. Soc.*, 2011, **133**, 4754; (b) H. Ming, Z. Ma, Y. Liu, K. M. Pan, H. Yu, F. Wang and Z. Kang, *Dalton Trans.*, 2012, **41**, 9526; (c) H. C. Zhang, H. Ming, S. Y. Lian, H. Huang, H. T. Li, L. L. Zhang, Y. Liu, Z. H. Kang and S. T. Lee, *Dalton Trans.*, 2011, **40**, 10822; (d) H. T. Li, R. H. Liu, Y. Liu, H. Huang, H. Yu, H. Ming, S. Y. Lian, S. T. Lee and Z. H. Kang, *J. Mater. Chem.*, 2012, **22**, 17470; (e) Y. Li, B. P. Zhang, J. X. Zhao, Z. H. Ge, X. K. Zhao and L. Zou, *Appl. Surf. Sci.*, 2013, **279**, 367; (f) Y. Liu, Y. X. Yu, W. D. Zhang, *J. Alloys Comp.*, 2013, **569**, 102.
- 9 (a) H. T. Li, X. D. He, Z. H. Kang, H. Huang, Y. Liu, J. L. Liu, S. Y. Lian, C. H. A. Tsang, X. B. Yang and S. T. Lee, *Angew. Chem., Int. Ed.*, 2010, **49**, 4430; (b) H. Li, R. Liu, S. Lian, Y. Liu, H. Huang and Z. Kang, *Nanoscale*, 2013, **5**, 3289.
- 10 (a) J. Ge, Q. Zhang, T. Zhang and Y. Yin, *Angew. Chem., Int. Ed.*, 2008, **47**, 8924; (b) Y. H. Deng, D. W. Qi, C. H. Deng, X. M. Zhang and D. Y. Zhao, *J. Am. Chem. Soc.*, 2008, **130**, 28; (c) B. Y. Yu and S. Y. Kwak, *J. Mater. Chem.*, 2012, **22**, 8345.
- 11 (a) H. Wang, J. Shen, Y. Y. Li, Z. Wei, G. Cao, Z. Gai, K. L. Hong, P. Banerjee and S. Q. Zhou, *Biomater. Sci.*, 2014, **2**, 915; (b) H. Wang, J. Shen, Y. Y. Li, Z. Wei, G. Cao, Z. Gai, K. L. Hong, P. Banerjee and S. Q. Zhou, *ACS Appl. Mater. Interfaces*, 2013, **5**, 9446.
- 12 (a) A. C. Ferrari and J. Robertson, *Phys. Rev. B*, 2000, **61**, 14095; (b) J. Ristein, R. T. Stief, L. Ley and W. Beyer, *J. Appl. Phys.*, 1998, **84**, 3836.
- 13 (a) S. J. Yu, M. W. Kang, H. C. Chang, K. M. Chen and Y. C. Yu, *J. Am. Chem. Soc.*, 2005, **127**, 17604; (b) Y. R. Chang, H. Y. Lee, K. Chen, C. C. Chang, D. S. Tsai, C. C. Fu, T. S. Lim, Y. K. Tzeng, C. Y. Fang, C. C. Han, H. Chang and W. Fan, *Nat. Nanotechnol.*, 2008, **3**, 284.
- 14 P. Duffy, L. Magno, R. Yadav, S. K. Roberts, A. D. Ward, S. W. Botchway, P. E. Colavita and S. J. Quinn, *J. Mater. Chem.*, 2012, **22**, 432.
- 15 F. Wang, S. P. Pang, L. Wang, Q. Li, M. Kreiter and C. Y. Liu, *Chem. Mater.*, 2010, **22**, 4528.
- 16 H. Wang, F. Ke, A. Mararenko, Z. Wei, Probal Banerjee and Shuiqin Zhou, *Nanoscale*, 2014, **6**, 7443.
- 17 Y. Yao, G. H. Li, S. Ciston, R. M. Lueptow and K. A. Gray, *Environ. Sci. Technol.*, 2008, **42**, 4952.
- 18 (a) S. Sakthivel, S. U. Geissen, D. W. Bahnemann, V. Murugesan and A. Vogelppohl, *J. Photochem. Photobiol. A*, 2002, **148**, 283; (b) J. G. Yu, X. X. Yu, B. B. Huang, X. Y. Zhang and Y. Dai, *Cryst. Growth Des.*, 2009, **9**, 1474; (c) W. Yan, H. Q. Fan and C. Yang, *Mater. Lett.*, 2011, **65**, 1595.